Annals of Nuclear Medicine Vol. 9, No. 4, 191–198, 1995

Validation of noninvasive quantification of rCBF compared with dynamic/integral method by using positron emission tomography and oxygen-15 labeled water

H. WATABE,* M. ITOH,** M. MEJIA R.,** T. FUJIWARA,** T. JONES*** and T. NAKAMURA**

*Department of Investigative Radiology, National Cardiovascular Center Research Institute, Osaka, Japan
**Cyclotron and Radioisotope Center, Tohoku University, Sendai, Japan
***MRC Cyclotron Unit, Hammersmith Hospital, London, U.K.

This study proposes a new solution for the quantification of rCBF pixel-by-pixel using PET and ^{15}O-H_2O. The method represents an application of weighted integration that uses PET image only, requiring no input function of arterial blood. It generates the rCBF image quickly and automatically. Simulation studies revealed that the calculation of rCBF was fairly stable as long as a relatively shorter scan frame time and longer scan time were selected. Calculated images of actual PET study by this method correlated significantly with those identified by the dynamic/integral method. Because this procedure could detect whole brain CBF change between different studies as accurately as by the dynamic/integral method, this procedure may be the most suitable for brain activation studies.

Key words: ^{15}O-labeled water, regional cerebral blood flow, positron emission tomography, noninvasive quantification

INTRODUCTION

INVESTIGATORS have devised several techniques for calculating rCBF by means of PET i.e., steady-state,[1] weighted integration,[2] autoradiographic[3, 4] and build-up technique,[5, 6] but in these models repeated arterial blood sampling in which the value is 100–200 m*l* in several runs is necessary to obtain absolute blood flow. The continuous measurement of arterial blood by tube, with a radiocounting device (β detector), should take into account delay and dispersion in the blood curve obtained relative to the brain data.[7] This procedure creates unnecessary complications for both subjects and examiners. Our study proposes a new numerical solution for rCBF calculation by using PET and O-15 labeled water.

In this paper, results of simulation studies and PET studies are presented. The theory of this method is shown in the appendix.

Received March 10, 1995, revision accepted June 7, 1995.

For reprint contact: H. Watabe, M.D., Department of Investigative Radiology, National Cardiovascular Center Research Institute, 5 Fujishiro-dai, Suita, Osaka 565, JAPAN.

MATERIAL AND METHODS

Simulations

With the following equation, tissue time-activity curves (TACs) were generated by using actual arterial input function and having the distribution volume fixed at 0.95:

$$C_t(T) = e^{-(f/V_d+\lambda)T} \cdot f \cdot \int_0^T C_a(t) \cdot e^{(f/V_d+\lambda)t} dt \quad (1)$$

Blood flow of 50 m*l*/100 g/min was used for Region 1, and by varying flow values from 20 to 100 m*l*/100 g/min, TACs for Region 2 were generated. Computation of Eq. (13) and (15) for the TACs of Region 1 and Region 2 gave estimations of flow for Region 2.

The accuracy and effects of scan protocol were evaluated by comparing the calculated values with the original ones used to generate tissue data.

In order to evaluate the effects of total scan time on the calculated rCBF, sequential tissue data at 5 sec interval in Regions 1 and 2 were generated up to 300 sec for flow values from 20 to 100 m*l*/100 g/min. With these tissue data, rCBF values at Region 2 were calculated by means of Eq. (14) (Fig. 2).

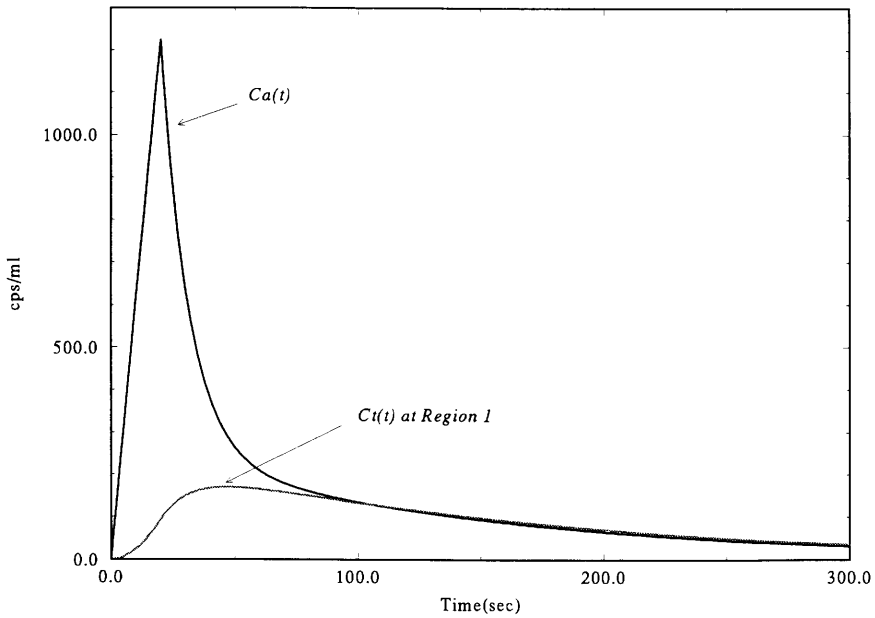

Fig. 1 Assumed input function and tissue activity curve at Region 1 as reference region. These curves were used in simulation studies. The input function was obtained from the measured data using β detector, by fitting to line for the initial part and two exponentials for the later part. The tissue activity curve are calculated from this input function assuming rCBF = 50 m*l*/100 g/min, $V_d = 0.95$.

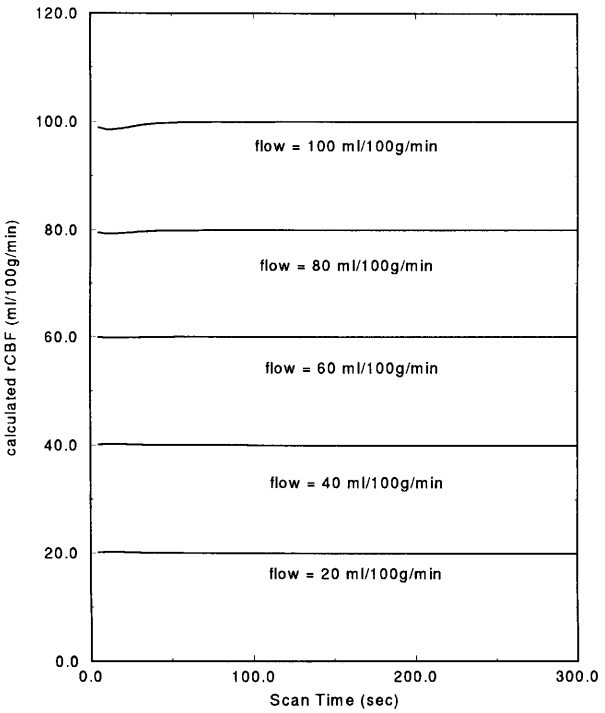

Fig. 2 The effects of PET scan time on calculations of rCBF. Calculated flows at Region 2 were plotted against PET scan time changing flows in Region 2 from 20 to 100 m*l*/100 g/min. Scan frame time is 5 sec.

In order to evaluate the effects of the frame time, it was varied from 5 sec to 100 sec. After generating tissue data at Region 2 for flow values from 20 m*l*/100 g/min to 80 m*l*/100 g/min, we calculated rCBF in Region 2 with the PET scan time fixed at 90 sec, 150 sec and 300 sec.

The evaluation of the effect of the fixed distribution volume has been done. Tissue data in Region 2 were generated with a flow range from 1 to 100 m*l*/100 g/min with three different V_d values: 0.85, 0.95 and 1.05. Scan frame time and scan time were fixed at 5 and 150 sec, respectively.

To evaluate the effect of noise on PET data, the random noise in the ± 30% range was added to the tissue data for each second for Regions 1 and 2. The rCBF was calculated for Region 2 with a 10 sec frame time.

The simulations were carried out on a workstation (SparcStation IPX; Sun Microsystems, Mountain View, CA, U.S.A.).

PET studies

In order to validate the method, a comparison between the present method and the dynamic/integral method[6] was carried out with actual PET data. PET studies with $C^{15}O_2$ inhalation on 17 normal volunteers (age: 20–59, mean 40.8 ± 14) were performed. Data were acquired with an ECAT 931-08/12 (CTI, Knoxville, TN, U.S.A.) positron emission scanner.[10]

Before 2 min dynamic $C^{15}O_2$ scan, a transmission scan was performed with external $^{67}Ge/^{68}Ga$ ring sources for tissue attenuation correction purposes. Dynamic scans were collected by means of the following protocol: 1 (background) frame of 30s, 4 of 5s, and 16 of 10s. Subjects inhaled a constant supply of $C^{15}O_2$ for a period of 2 min beginning at the start of the second frame through

a face mask. Arterial blood radioactivity was measured with an on-line detection system. Blood was withdrawn continuously through a radial artery cannula at a speed of 5 m*l*/min with polyethene tubing (length 65 cm from cannula to scintillation crystal) with an internal diameter of 1 mm and a wall thickness of 0.5 mm. For each study scanning started when all tubing components were filled with blood after blood had been withdrawn. Four minutes after the start of scanning, one 2 m*l* calibration sample was collected through a three-way tap positioned directly behind the BGO scintillator. Following the collection of this calibration sample, the whole-blood circuit (including the cannula) was flushed with heparinised saline.

All emission scans were reconstructed with a Hanning filter with a cut-off frequency of 0.5 of maximum, which resulted in a spatial resolution of 8.4 × 8.3 × 6.6 mm full width at half-maximum at the center of the field of view.[10]

Image processing

The reconstructed dynamic images were transferred to the SparcStation for image processing.

Programs were developed which calculated rCBF by pixel-base for the two different methods—the present method and the dynamic/integral method. The steps in our method are as follows:

1. Generation of single and double integration images,

   i.e., $\int C_t, \int\int C_t, \int C_t^*, \int\int C_t^*$
2. Pixels within 10% of the highest value in the integrated images were determined and averaged to create the time activity curves in the Region 1.
3. Calculation of the flows in Region 1 taking all pixels as Region 2s. Then the flow for Region 1 was fixed at the mean of these values.
4. Calculation of flows at each pixel in Region 2.

Another set of rCBF images were calculated by the dynamic/integral method.[6] Whole-brain ROIs were defined on planes 6 to 10 of the 15 planes of integrated images, created by summing counts of all frames over the 2 min inhalation period. By projecting these ROIs on the 21 dynamic frames and averaging over the 5 planes, the time activity curve of the whole-brain was generated. This curve was used to determine delay and dispersion of the arterial whole-blood curve.[6] A rCBF vs $\int C_t$ lookup table was generated by using the determined delay (d), dispersion (p), and fixed V_d (0.95) as follows[5]:

$$\int_{T_1}^{T_2} Ct(t)dt = \frac{f\left\{\left(\frac{f}{V_d}-p\right)\int_{T_1+d}^{T_2+d} C_m(t)\otimes\exp\left[-\left(\frac{f}{V_d}+\lambda\right)t\right]dt + (p+\lambda)\int_{T_1+d}^{T_2+d} C_m(t)dt\right\}}{p\left(\frac{f}{V_d}+\lambda\right)} \quad (2)$$

where ⊗ denotes the operation of convolution, T_1 is frame start time, T_2 is frame end time and $C_m(t)$ is the measured arterial curve. The rCBF images were generated by using this lookup table.

RESULTS

An evaluation was made of the effects of total scan time on the calculated rCBF. At shorter scan time calculated flows were overestimated when the flow value was lower than the flow in Region 1 (50 m*l*/100 g/min) and underestimated when flow value was higher than 50 m*l*/100 g/min, but amounts of over- or underestimation were lower than 1%, and rCBF values became asymptotic after a 10 sec scan. These trends were similar for all flow values.

The effects of the frame time are shown in Figure 3. As shown in Figure 3 errors were increased with longer scan frame time. In the case of 20 m*l*/100 g/min (lower than the flow in Region 1) calculated flows were overestimated. On the other hand, in the case of 80 m*l*/100 g/min calculations were underestimated. When scan time was longer, the calculation gave a better estimation of flow less dependent on the scan frame time. For example at a 50 sec frame time, errors in calculation for flow 20 m*l*/100 g/min were 16% (90 sec scan time), 1.7% (150 sec scan time) and 0.1% (300 sec scan time).

The effect of the fixed distribution volume is shown in Figure 4. Figure 4 illustrates the rCBF errors due to incorrect distribution volume. The distribution volume of 0.85 generates singular values around 50 m*l*/100 g/min (flow value in Region 1), although appropriate agreements were obtained between true and calculated values at a lower flow level. With a higher flow, the calculated values tended to be higher than the true values (calculated values were 4.4% higher on average than true values at a flow level of 60 to 100 m*l*/100 g/min). A larger distribution volume, for example 1.05, underestimates the flow, especially in a higher flow region (1.0% underestimation of flow at 60–100 m*l*/100 g/min). Singular deviations were also found around 50 m*l*/100 g/min.

The noise effect has been examined in Figure 5. A higher noise level produced larger errors in the calculated values, as shown in Figure 5, but the longer scan time and lower flow regions were less dependent on noise.

For each subject, the images obtained with both methods were compared by plotting rCBF values for regions of 4 × 4 pixels in all planes against each other. Regression curves and correlation coefficient were calculated for all studies and are shown in Table 1. The mean value was calculated by averaging all individual pixels in all slices. In order to remove the pixels out of the brain from the calculation of mean value, the transmission images were used for masking the brain field. The mean value was slightly lower than the typical value, 50 m*l*/100 g/min, because some pixels are outside of the brain. Figure 6 shows the mean CBF values calculated by both methods

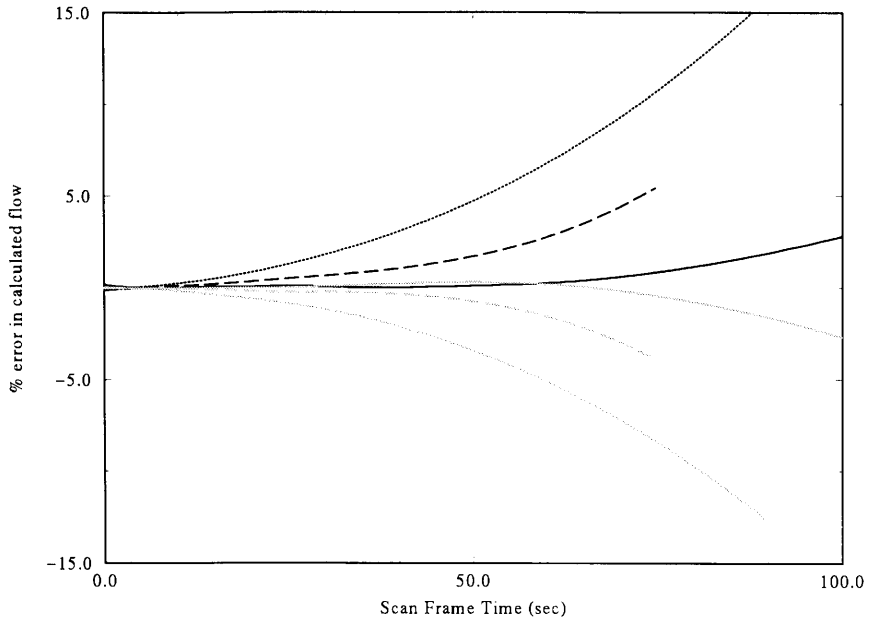

Fig. 3 The effects of scan frame time on calculations of rCBF. Percentage of errors of calculated flows against true flows were plotted as a function of interval of PET scanning. Solid, dashed, and dot lines indicate scan time for 300 sec, 150 sec and 90 sec, respectively. Black and gray lines indicate true flows of 20 ml/100 g/min and 80 ml/100 g/min, respectively.

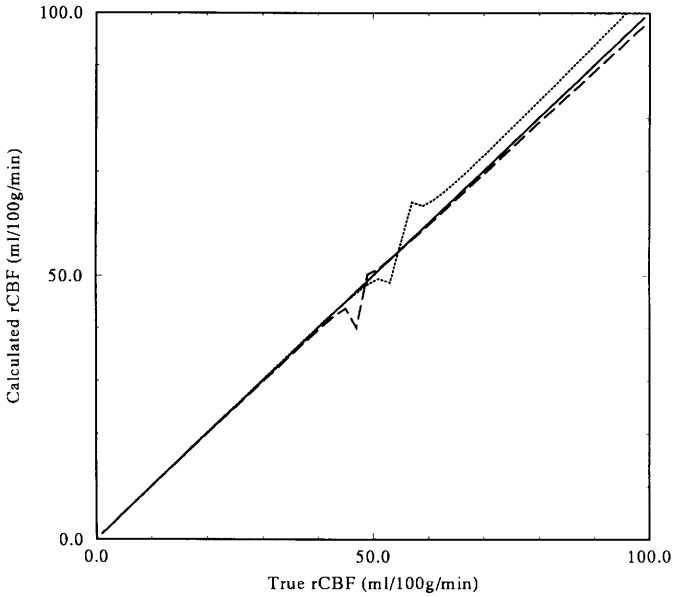

Fig. 4 Errors due to incorrect distribution volume. Combinations of true rCBF vs. calculated rCBF are plotted. Solid line, dashed line and dotted line indicate distribution volume to be 0.95, 1.05 and 0.85, respectively. Scan frame time is 5 sec.

Table 1 Comparison of two methods

Run No.	mean[1]	mean[2]	cor. coef.	slope	intercept
p1414	27.0	33.1	1.00	1.25	−0.565
p1474	28.9	33.6	1.00	1.18	−0.341
p1597	24.9	33.8	1.00	1.39	−0.894
p1634	29.9	33.1	1.00	1.11	0.014
p1639	26.1	36.8	1.00	1.45	−1.06
p1644	36.7	33.7	1.00	0.91	0.398
p1657	33.7	32.5	1.00	0.96	0.219
p1672	27.0	36.6	1.00	1.39	−0.881
p1770	24.3	33.6	1.00	1.41	−0.763
p1803	23.1	28.6	1.00	1.26	−0.435
p1831	38.3	32.1	1.00	0.82	0.642
p1852	25.1	31.1	1.00	1.26	−0.391
p1865	25.7	30.1	1.00	1.18	−0.232
p1949	28.7	37.3	1.00	1.33	−0.698
p2018	36.2	40.9	1.00	1.14	−0.331
p2037	33.1	37.1	1.00	1.13	−0.278
p2122	33.4	38.9	1.00	1.18	−0.523
Average	29.5	34.3	1.00	1.20	−0.360
SD	4.8	3.2	1×10^{-4}	0.180	0.466

[1]mean CBF value (ml/100 g/min) of whole brain image by dynamic/integral method

[2]mean CBF value (ml/100 g/min) of whole brain image by the present method

for all subjects. When data for p1644, p1657 and p1831 were excluded, the correlation coefficient was 0.788, with a significant correlation between the two methods (paired t test $p < 0.0005$).

DISCUSSION

The present technique is based on weighted integration,[8] and has the following characteristics:

- The method is noninvasive, requiring no arterial input

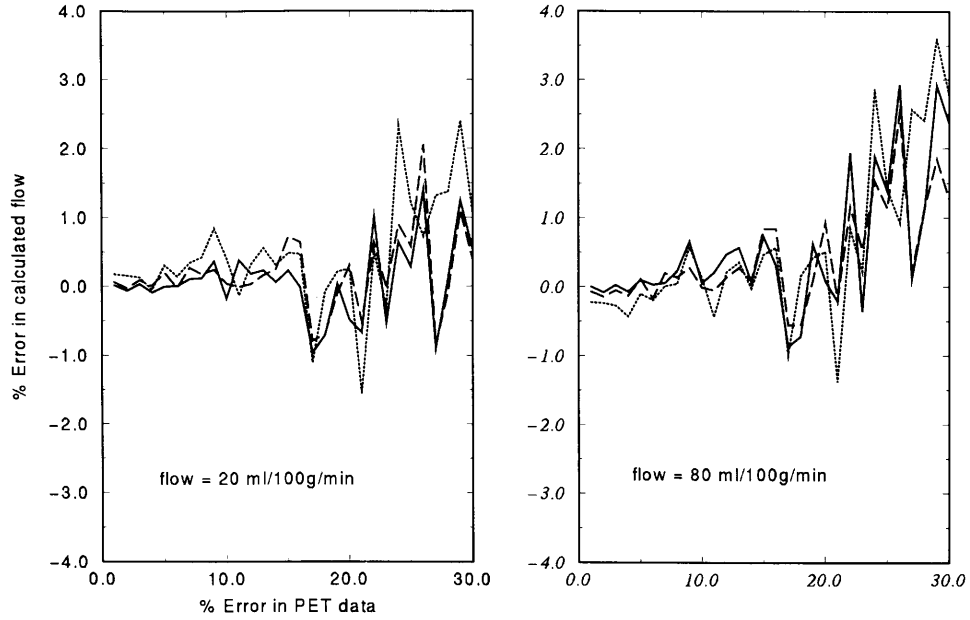

Fig. 5 Simulation of errors due to statistical noise. Random noises were added to tissue counts at amount of 1 to 30% of the count. Simulations were performed on lower flow value, 20 ml/100 g/min (left) or higher flow value, 80 ml/100 g/min (right).

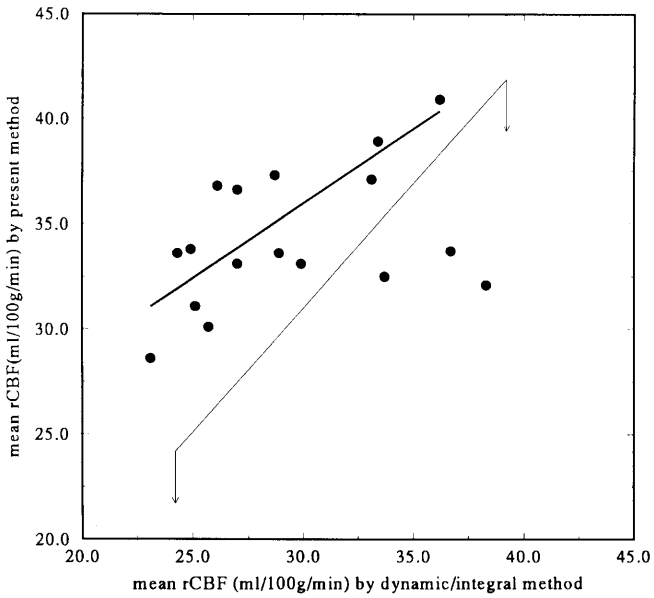

Fig. 6 Comparisons of mean rCBF values of 17 subjects calculated by the dynamic/integral method (abscissa) and the present method (ordinate) with a regression curve. Data below a line with arrows are omitted for calculation of regression.

function and hence corrections for dispersion and time delay. No arterial counting devices are necessary.

- The method produces pixel-by-pixel, functional images of rCBF with short calculation time.
- The calculations proceed automatically without the operator's intervention.

Once the feasibility of mapping human brain function by means of PET was established, numerous research designs were developed. The localization of cortical centers for the processing of stimuli such as tactile, visual, auditory, etc. was a prime focus, but since PET measurement studies require a relatively long time period to complete (in the order of minutes), the state of attention relative to habituation has became problematic. The subject's psychological state is often disturbed. Arterial blood sampling taken during PET studies can be stressful, so that it is often omitted and replaced by the standard

input function; but this simplified method cannot give absolute flow changes before and after stimulation. The standard input function can be a good estimation of true individual input only when the time difference or time delay between the standard and brain curve is correctly known. Moreover, the difference in circulation time of H_2O in large vessels in individual subjects easily distorts the profile of the arterial curve. This technique may therefore sometimes enhance the non-lineality of the PET count further. The present noninvasive procedure was developed to solve the above problems simultaneously and practically with the additional advantage of efficient, automatic calculation.

The method presented in this paper is based on the weighted integration methods, which uses two types of PET data—one, decay-corrected and the other without decay-correction. The weighted integration method was originally utilized by Huang et al.[8] and Alpert et al.[11] Their purpose was to shorten calculation time while improving accuracy. Their techniques required arterial input function. Our report may therefore be the first that uses true, noninvasive CBF measurement with ^{15}O-water.

Gambhir et al.[12] reported that CBF values derived by the integrated projection technique depended on scan time, implying that delay and dispersion were not taken into account in the measured arterial blood curve. Our technique is, in principle, free from these problems. According to our first simulation, the rCBF value did not depend on the PET scan time. Errors in calculation with a shorter scan time may be due to errors in numerical integrations caused by discrete data sampling. It is known that the trapezoidal rule of integration sometimes produces errors, especially in the ascendant phase of curve formation.

This technique calculates rCBF in two regions simultaneously, in which input functions in both regions are assumed to be the same. Region 1 was fixed at in certain area as a reference and the flow in Region 2 (each of the all pixels) was compared with that in Region 1. One of the problems is the selection of the reference region. Because it is better to work with homogeneous tissue, such as gray matter, 10% maximum counts of the integrated image were selected. With this setting, the program can proceed automatically. Optimization of the selection of the referece region must be done.

The assumption is that all brain tissue has the same distribution volume. As indicated in the simulation, this assumption leads to large errors, especially in the calculation of flow that is close to that of Region 1. Subtractions as $\left(\int\int C_{t_1} - \int\int C_{t_2}\right)$ in the denominator in equations such as Eq. (15) may induce relatively larger errors from minor errors in $C_t(t)$. This may explain the oscillation around the flow value of 50 ml/100 g/min in Figure 4.

In spite of the above problems, correlation between our method and the dynamic/integral method in PET studies was fairly good except for tree excluded data (Fig. 6). We have not found the differences between the three excluded data and others in Figure 6. Further studies will be required.

The results of simulations revealed that a shorter scan frame time could reduce errors in calculation, but by a choosing longer scan time this error can be canceled. By limiting the injected dose as well as limiting the sensitivity of the PET scanner, it is possible to select an optimum scan time and scan intervals to make possible precise measurement of rCBF.

In conclusion, this procedure proposes a new solution for rCBF calculation by using ^{15}O-water injection. The method is noninvasive since no blood sampling is required. The calculation is relatively simple and can generate the rCBF image quickly on completion of PET scans.

APPENDIX

The model applied the single compartment model originally developed by Kety,[9] in which the differential equation for the tissue radioactive concentration and arterial input function as follows:

$$\frac{dC_t(t)}{dt} = fC_a(t) - \left(\frac{f}{V_d} + \lambda\right)C_t(t) \tag{3}$$

(Note: Where $C_t(t)$ and $C_a(t)$ reflect the tissue radioactive concentration values at time t in the brain and arterial blood respectively, f is the regional cerebral blood flow, V_d is the distribution volume of water and λ is the physical decay constant for ^{15}O—half life is 122 sec). Another differential equation for the decay-corrected data is:

$$\frac{dC_t^*(t)}{dt} = fC_a^*(t) - \frac{f}{V_d}C_t^*(t) \tag{4}$$

the data with the superscripted asterisks are decay corrected. Choosing any 2 regions called Regions 1 and 2 in the brain, Eq. (1) and (2) can be applied to Region 1 or Region 2, as follows:

$$\frac{dC_{t_1}(t)}{dt} = f_1C_a(t) - \left(\frac{f_1}{V_d} + \lambda\right)C_{t_1}(t) \tag{5}$$

$$\frac{dC_{t_2}(t)}{dt} = f_2C_a(t) - \left(\frac{f_2}{V_d} + \lambda\right)C_{t_2}(t) \tag{6}$$

$$\frac{dC_{t_1}^*(t)}{dt} = f_1C_a^*(t) - \frac{f_1}{V_d}C_{t_1}^*(t) \tag{7}$$

$$\frac{dC_{t_2}^*(t)}{dt} = f_2C_a^*(t) - \frac{f_2}{V_d}C_{t_2}^*(t) \tag{8}$$

The data with the subscripted numbers are from the specified regions. It is reasonable to assume that the input function $C_a(t)$ was the same for all brain regions, and the

distribution volume V_d may be fixed for every pixel at 0.95 ml/g. [6] Thus, two time integrations of the four equations above, during time 0 to T yield:

$$\int_0^T C_{t_1}(t)dt = f_1 \int_0^T dt \int_0^t C_a(s)ds - \left(\frac{f_1}{V_d} + \lambda\right) \int_0^T dt \int_0^t C_{t_1}(s)ds \quad (9)$$

$$\int_0^T c_{t_2}(t)dt = f_2 \int_0^T dt \int_0^t C_a(s)ds - \left(\frac{f_2}{V_d} + \lambda\right) \int_0^T dt \int_0^t C_{t_2}(s)ds \quad (10)$$

$$\int_0^T C^*_{t_1}(t)dt = f_1 \int_0^T dt \int_0^t C^*_a(s)ds - \frac{f_1}{V_d} \int_0^T dt \int_0^t C^*_{t_1}(s)ds \quad (11)$$

$$\int_0^T C^*_{t_2}(t)dt = f_2 \int_0^T dt \int_0^t C^*_a(s)ds - \frac{f_2}{V_d} \int_0^T dt \int_0^t C^*_{t_2}(s)ds \quad (12)$$

$$\int_0^T C_{t_1}(t)dt = \frac{f_1}{f_2}\left\{\int_0^T C_{t_2}(t)dt + \left(\frac{f_2}{V_d} + \lambda\right) \int_0^T dt \int_0^t C_{t_2}(s)ds\right\} - \left(\frac{f_1}{V_d} + \lambda\right) \int_0^T dt \int_0^t C_{t_1}(s)ds \quad (13)$$

$$\int_0^T C^*_{t_1}(t)dt = \frac{f_1}{f_2}\left\{\int_0^T C^*_{t_2}(t)dt + \frac{f_2}{V_d} \int_0^T dt \int_0^t C^*_{t_2}(s)ds\right\} - \frac{f_1}{V_d} \int_0^T dt \int_0^t C^*_{t_1}(s)ds \quad (14)$$

From Eq (11) and Eq (12), flow f_1 and f_2 for Regions 1 and 2, respectively, can be rewritten:

$$f_1 = \frac{V_d\left\{\begin{array}{l}\int_0^T C_{t_1}(t)dt \int_0^T C^*_{t_2}(t)dt - \int_0^T C^*_{t_1}(t)dt \int_0^T C_{t_2}(t)dt \\ +\lambda \int_0^T C^*_{t_2}(t)dt \int_0^T dt \int_0^t C_{t_1}(s)ds \\ -\lambda \int_0^T C^*_{t_1}(t)dt \int_0^T dt \int_0^t C_{t_2}(s)ds\end{array}\right\}}{\left\{\begin{array}{l}\int_0^T C_{t_2}(t)dt\left(\int_0^T dt \int_0^t C^*_{t_1}(s)ds - \int_0^T dt \int_0^t C^*_{t_2}(s)ds\right) \\ +\int_0^T C^*_{t_2}(t)dt\left(\int_0^T dt \int_0^t C_{t_2}(s)ds - \int_0^T dt \int_0^t C_{t_1}(s)ds\right) \\ +\lambda \int_0^T dt \int_0^t C_{t_2}(s)ds\left(\int_0^T dt \int_0^t C^*_{t_1}(s)ds - \int_0^T dt \int_0^t C^*_{t_2}(s)ds\right)\end{array}\right\}} \quad (15)$$

$$f_2 = \frac{V_d\left\{\begin{array}{l}\int_0^T C_{t_1}(t)dt \int_0^T C^*_{t_2}(t)dt - \int_0^T C^*_{t_1}(t)dt \int_0^T C_{t_2}(t)dt \\ +\lambda \int_0^T C^*_{t_2}(t)dt \int_0^T dt \int_0^t C_{t_1}(s)ds \\ -\lambda \int_0^T C^*_{t_1}(t)dt \int_0^T dt \int_0^t C_{t_2}(s)ds\end{array}\right\}}{\left\{\begin{array}{l}\int_0^T C_{t_1}(t)dt\left(\int_0^T dt \int_0^t C^*_{t_1}(s)ds - \int_0^T dt \int_0^t C^*_{t_2}(s)ds\right) \\ +\int_0^T C^*_{t_1}(t)dt\left(\int_0^T dt \int_0^t C_{t_2}(s)ds - \int_0^T dt \int_0^t C_{t_1}(s)ds\right) \\ +\lambda \int_0^T dt \int_0^t C_{t_1}(s)ds\left(\int_0^T dt \int_0^t C^*_{t_1}(s)ds - \int_0^T dt \int_0^t C^*_{t_2}(s)ds\right)\end{array}\right\}} \quad (16)$$

With positron tomography, the counts are the integrals $\int C_{t1}(t)dt$ and $\int C_{t2}(t)dt$. Sampling the data without decay-correction, the decay corrections were carried out numerically on reconstracted images. The double integrations $\int\int C_t$ and $\int\int C_t$ were calculated by means of the numerical integrations by applying the trapezoidal rule. For the actual calculation, Region 1 (reference region) was selected as 10% of the maximum value for integrated images. By taking each of the brain pixels as those for Region 2, the flows for Region 1 were obtained by Eq. (13). The actual rCBF value for Region 1 was estimated by averaging these values for each pixel. Then the flow for each pixel (p) was calculated from the following equation derived from Eq. (12).

$$f_p = \frac{\int_0^T C^*_{t_p}(t)dt}{\frac{1}{f_1}\int_0^T C^*_{t_1}(t)dt + \frac{1}{V_d}\int_0^T dt \int_0^t C^*_{t_1}(s)ds - \frac{1}{V_d}\int_0^T dt \int_0^t C^*_{t_p}(s)ds} \quad (17)$$

REFERENCES

1. Frackowiak RSJ, Lenzi GL, Jones T, Heather JD. Quantitative measurement of regional cerebral blood flow and oxygen metabolism in man using ^{15}O and positron emission tomography: theory, procedure, and normal values. *J Comput Assist Tomogr* 4: 727–736, 1980.
2. Huang SC, Carson RE, Hoffman EJ, Carson J, MacDonald N, Barrio JR, et al. Quantitative measurement of local cerebral blood flow in humans by positron computed tomography and ^{15}O-water. *J Cereb Blood Flow Metab* 3: 141–153, 1983.
3. Raichle ME, Martin WRW, Herscovitch P, Mintun MA, Markham J. Brain blood flow measured with intravenous $H_2{}^{15}O$. II. Implementation and validation. *J Nucl Med* 29: 241–247, 1983.
4. Kanno I, Lammertsma AA, Heather JD, Gibbs JM, Rhodes CG, Clark JC, et al. Measurement of cerebral blood flow using bolus inhalation of $C^{15}O_2$ and positron emission tomography: description of the method and its comparison with the $C^{15}O_2$ continuous inhalation method. *J Cereb Blood Flow Metab* 4: 224–234, 1984.
5. Lammertsma AA, Frackowiak RSJ, Hoffman JM, Huang SC, Weinberg IN, Dahlbom M, et al. The $C^{15}O_2$ build-up technique to measure regional cerebral blood flow and volume of distribution of water. *J Cereb Blood Flow Metab* 9: 461–470, 1989.
6. Lammertsma AA, Cunningham VJ, Deiber MP, Heather JD, Bloomfield PM, Nutt J, et al. Combination of Dynamic and Integral Methods for Generating Reproducible Functional CBF Images. *J Cereb Blood Flow Metab* 10: 675–686, 1990.
7. Iida H, Kanno I, Miura S, Murakami M, Takahashi K, Uemura K. Error analysis of a quantitative cerebral blood flow measurement using $H_2{}^{15}O$ autoradiography and positron emission tomography, with respect to the dispersion of the input function. *J Cereb Blood Flow Metab* 6: 536–545, 1986.
8. Huang SC, Carson RE, Phelps ME. Measurement of local blood flow and distribution volume with short-lived isotopes: A general input technique. *J Cereb Blood Flow Metabol* 2: 99–108, 1982.
9. Kety SS. The theory and applications of the exchange of inert gas at the lungs and tissues. *Pharmacol Rev* 3: 1–41, 1951.
10. Spinks TJ, Jones T, Gilardi MC, Heather JD. Physical performance of the latest generation of commercial positron scanner. *IEEE Trans Nucl Sci* NS 35: 721–725, 1988.
11. Alpert NM, Eriksson L, Chang JY, Bergstrom M, Litton JE, Correia JA, et al. Strategy for the measurement of regional

cerebral blood flow using short-lived tracers and emission tomography. *J Cereb Blood Flow Metab* 4: 28–34, 1984.
12. Gambhir SS, Huang SC, Hawkins RA, Phelps ME. A study of the single compartment tracer kinetic model for the measurement of local cerebral blood flow using ^{15}O-water and positron emission tomography. *J Cereb Blood Flow Metab* 7: 13–20, 1987.